Reflection of Ocean Surface Gravity Waves from a Natural Beach

STEVE ELGAR

School of Electrical Engineering and Computer Science, Washington State University, Pullman, Washington

T. H. C. HERBERS* AND R. T. GUZA

Center for Coastal Studies, Scripps Institution of Oceanography, La Jolla, California

(Manuscript received 28 May 1993, in final form 24 September 1993)

ABSTRACT

The energy of seaward and shoreward propagating ocean surface gravity waves on a natural beach was estimated with data from an array of 24 bottom-mounted pressure sensors in 13-m water depth, 2 km from the North Carolina coast. Consistent with a parameterization of surface wave reflection from a plane sloping beach by Miche, the ratio of seaward to shoreward propagating energy in the swell–sea frequency band (0.044–0.20 Hz) decreased with increasing wave frequency and increasing wave height, and increased with increasing beach-face slope. Although most incident swell–sea energy dissipated in the surf zone, reflection was sometimes significant (up to 18% of the incident swell–sea energy) when the beach face was steep (at high tide) and the wave field was dominated by low-energy, low-frequency swell. Frequency–directional spectra show that reflection of swell and sea was approximately specular. The ratio of seaward to shoreward propagating energy in the infragravity frequency band (0.010–0.044 Hz) varied between about 0.5 and 3 and increased with increasing swell energy. This trend suggests that infragravity waves generated in very shallow water, and refractively trapped on the sloping seabed, are significantly dissipated over a 50-km wide shelf during storms.

1. Introduction

Shoreward propagating surface gravity waves evolve substantially in shallow water owing to refraction, shoaling, nonlinear interactions, and dissipation. Usually, most of the incident wave energy is dissipated by wave breaking in the surf zone, but under some conditions reflection back toward deep water is significant. Reflection of surface waves from ocean beaches is poorly understood. In the present study, estimates of the ratio R^2 of seaward to shoreward propagating wave energy are used to investigate reflection from a natural beach. Miche (1951) empirically determined that, for monochromatic waves normally incident on a plane laboratory beach,

$$R^2 \approx 1 \quad \text{when} \quad M = \frac{16g^2}{(2\pi)^5}\frac{\tan^5\beta}{H_\infty^2 f^4} \geq 1, \quad (1a)$$

where M will be called the Miche number; β is the beach slope; H_∞ and f are the deep water wave height and wave frequency, respectively; and g is the gravitational acceleration. Carrier and Greenspan (1958) obtained theoretically a similar result (within a factor of 2) based on the nonlinear, inviscid, shallow-water equations (see also Munk and Wimbush 1969 and Meyer and Taylor 1972). Miche (1951) suggested that

$$R^2 \approx M \quad \text{when} \quad M < 1, \quad (1b)$$

with the remainder of the energy dissipated through wave breaking.

Results of laboratory experiments with monochromatic waves are qualitatively consistent with Eq. (1) (e.g., Moraes 1970; Guza and Bowen 1976; Mansard and Funke 1980; Guza et al. 1984, and references therein). Field studies of reflection from natural beaches are limited. Tatavarti et al. (1988) and Walton (1992) used collocated velocity and pressure measurements near the shoreline at several field sites to estimate shoreward and seaward propagating wave energy. The observed R^2 followed the trends suggested by Eq. (1), but was small at swell–sea frequencies in all the datasets. Many studies (e.g., Suhayda 1974; Guza and Thornton 1985; Nelson and Gonsalves 1990; Walton 1992) have noted that R^2 is O(1) at infragravity frequencies (<0.05 Hz). However, the interpretation of these large R^2 estimates at low frequencies is complicated because infragravity waves are believed to be nonlinearly excited in very shallow water.

Accurate estimates of R^2 require detailed measurements of the directional wave properties, information

* Current affiliation: Department of Oceanography, Naval Postgraduate School, Monterey, California.

Corresponding author address: Dr. Steve Elgar, School of Electrical Engineering and Computer Science 2752, Washington State University, Pullman, WA 99164-2752.

not available in the field studies of Suhayda (1974), Nelson and Gonsalves (1990), and Walton (1992). Freilich and Guza (1984) and Herbers and Guza (1990) estimated reflection with observations from arrays of sensors in 4–10 m depth for a few datasets and concluded that less than 10% of the total swell and sea energy was propagating seaward. In the present study, R^2 was estimated with a more extensive dataset obtained from a 24-element, large-aperture array of pressure sensors in 13-m water depth. The field experiment and data analysis are briefly described in section 2, with additional detail in the appendix. Observations of R^2 in the swell–sea and infragravity frequency bands are discussed in section 3, where it is shown that reflection in the swell–sea frequency band is qualitatively consistent with Miche's hypothesis [Eq. (1b)]. The ratio of seaward to shoreward propagating infragravity energy was often greater than 1, and as high as 3 when swell–sea energy was maximum. The results are summarized in section 4.

2. Field experiment and data reduction

An array of 24 pressure sensors (Fig. 1a) was deployed on the sandy seafloor in 13-m water depth, 2 km offshore of the U.S. Army Corps of Engineers Field Research Facility at Duck, North Carolina (for details see Herbers et al. 1994a). The array site, offshore of a relatively straight barrier island, is exposed to ocean waves from a wide range of deep water propagation directions. The beach is concave (Fig. 1b, see also Birkemeier et al. 1992) and the beach-face slope β, defined as the mean slope of the portion of the beach face covered by a typical swash excursion [O(10 m) wide], ranged from 0.051 to 0.142, primarily owing to tidal fluctuations in sea level. The slope at the array site was about 0.005 (Fig. 1b) and small depth variations (<1 m) across the array are neglected here.

For the present study, 242 datasets (each 2 h, 50 min long and sampled at 4 Hz) collected during September–November 1990 and January 1991 were analyzed. Significant wave heights (four times the standard deviation of surface elevation fluctuations in the swell–sea frequency band, estimated from bottom pressure with a linear theory depth correction) ranged from 18 to 240 cm. Mean frequencies (corresponding to the centroid of the swell–sea surface elevation spectrum) ranged from 0.077 to 0.185 Hz. Spectral estimates reported here have a frequency resolution of 0.0068 Hz and about 150 degrees of freedom.

The datasets were collected within a few days of bathymetric surveys, which were obtained at least once or twice each month, and daily during the first three weeks of October 1990 (Birkemeier et al. 1992). Numerical simulations using an extension of the mild-slope equation (Kirby 1986, 1987) and the measured bathymetry indicate that swell and sea are not significantly reflected from the alongshore oriented sandbar

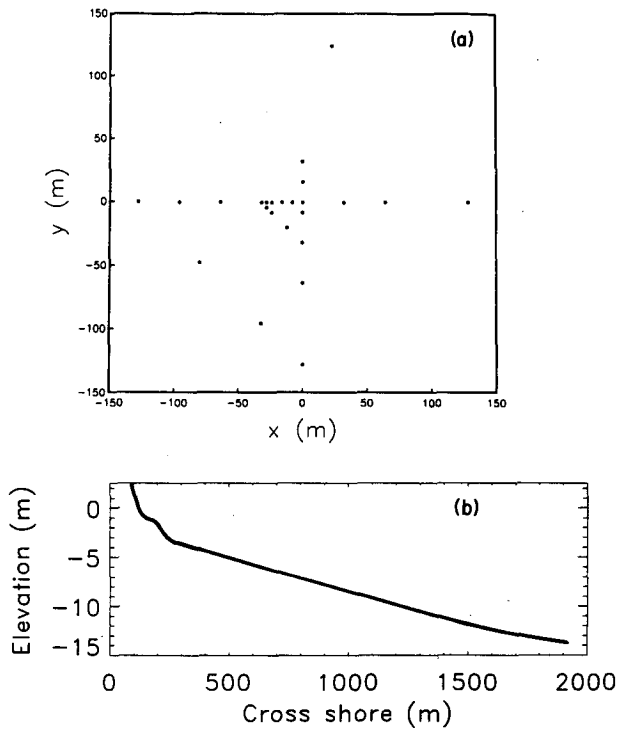

FIG. 1. (a) Plan view of the array of 24 pressure sensors in 13-m depth. The positive y axis points offshore, and the negative x axis points approximately north. (b) Seafloor profile between the pressure sensor array and the shoreline.

(in about 1.5-m water depth, Fig. 1b). Moreover, as discussed below, the reflection of swell and sea is typically largest at high tide when the sandbar is furthest below the sea surface, but the beach-face slope is steepest, consistent with reflection from the beach face rather than the sandbar.

The ratio of offshore to onshore propagating energy as a function of frequency, $R^2(f)$,

$$R^2(f) = \frac{E_{\text{off}}(f)}{E_{\text{on}}(f)} \tag{2a}$$

with

$$E_{\text{on}}(f) = \int_{180°}^{360°} E(f, \theta)\, d\theta \tag{2b}$$

$$E_{\text{off}}(f) = \int_{0°}^{180°} E(f, \theta)\, d\theta \tag{2c}$$

and $E(f, \theta)$ the frequency (f)–directional (θ) spectrum (90° and 270° correspond to offshore and onshore propagation, respectively), was estimated from each dataset using the method described in the Appendix.

The 250-m array aperture is several times larger than the wavelengths of swell and sea waves, and $E(f, \theta)$ is well resolved by the array in the swell–sea band. The array dimensions are comparable to (or less than) the

wavelengths of infragravity waves, and thus the directional resolution at these frequencies is lower. However, $R^2(f)$ [Eq. (2)] is a bulk moment of the directional wave field, and is insensitive to the fine structure of $E(f, \theta)$. The accuracy of the $R^2(f)$ estimates at both swell–sea and infragravity frequencies is demonstrated with model tests in the appendix.

3. Seaward- and shoreward-propagating waves

The average of all 242 energy spectra (each normalized by its total variance) is shown in Fig. 2a. The swell–sea and infragravity peaks at about $f = 0.10$ and 0.02 Hz, respectively, are separated by a spectral minimum near $f = 0.04$ Hz. Spectra observed at other shelf sites have similar average shapes (Herbers et al. 1994b).

The frequency dependence of $R^2(f)$ is shown in Fig. 2b. At infragravity frequencies $R^2(f)$ ranges from about 0.5 to 5.0. In the swell–sea frequency band $R^2(f)$ decreases rapidly with increasing frequency, and is usually below 0.1 for $f > 0.1$ Hz. Frequency-integrated (bulk) R^2 values were estimated for both the swell–sea (R^2_{ss}) and infragravity (R^2_{ig}) bands:

$$R^2_{ig} = \frac{\int_{0.010\text{Hz}}^{0.044\text{Hz}} E_{off}(f)\,df}{\int_{0.010\text{Hz}}^{0.044\text{Hz}} E_{on}(f)\,df} \tag{3a}$$

$$R^2_{ss} = \frac{\int_{0.044\text{Hz}}^{0.20\text{Hz}} E_{off}(f)\,df}{\int_{0.044\text{Hz}}^{0.20\text{Hz}} E_{on}(f)\,df}, \tag{3b}$$

where the separation frequency $f = 0.044$ Hz was chosen to avoid contamination of infragravity motions by more energetic swell (Fig. 2a). The results presented here are not greatly affected by the choice of a separation frequency in the range 0.037–0.051 Hz.

a. Swell–sea waves

The bulk R^2 for swell–sea, R^2_{ss}, decreases as the swell–sea energy increases (Fig. 3a). For wave fields with swell–sea energy greater than about 200 cm^2, $R^2_{ss} < 0.03$, about the minimum detectable level (appendix). For lower-energy wave fields, R^2_{ss} values as large as 0.18 were observed.

The reflection of swell–sea energy varied with beach slope. During the 3-day period shown in Fig. 4, the total energy and mean frequency of swell–sea were relatively low and constant, but the beach slope varied owing to tidal fluctuations of the mean water level on the approximately parabolically shaped beach face. For the data shown in Fig. 4, R^2_{ss} is roughly proportional to β^5, consistent with Eq. (1). Tidal modulation of R^2_{ss} was less apparent during other time periods with detectable reflection, possibly because of more variable swell–sea energy spectra.

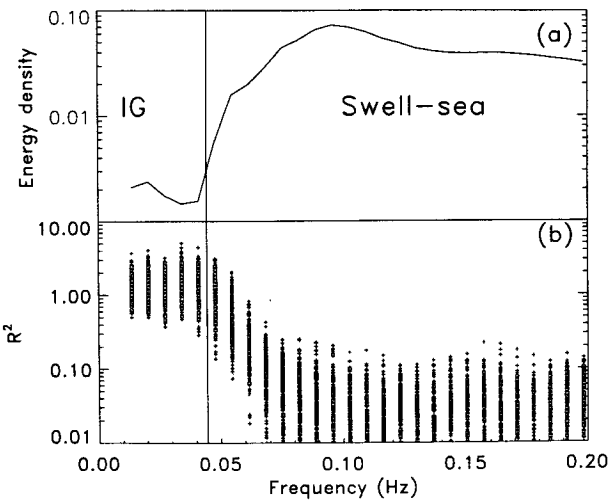

FIG. 2. (a) Average (over the 242 datasets) of normalized (by the total variance of each individual dataset) frequency spectra and (b) $R^2(f)$ [ratio of seaward to shoreward propagating energy, Eq. (2)] for the 242 datasets. The solid vertical line at $f = 0.044$ Hz indicates the separation of infragravity (IG) from swell and sea (SS) frequency bands.

The three parameters affecting reflection in the swell–sea band (frequency, Fig. 2; energy, Fig. 3; beach slope, Fig. 4) can be combined into the nondimensional Miche number, M [Eq. (1)]. The observed values of R^2_{ss} are well correlated with M (Fig. 5), where M is based on the significant wave height observed at the array, the centroidal frequency of the swell–sea band, and the beach slope as defined in section 2. This definition of M is somewhat arbitrary. For example, using root-mean-square wave height instead of significant wave height would offset the data in Fig. 5 by a factor of 2. Although Miche's empirical result is based on monochromatic waves on constant slope beaches, the present observations suggest that the reflection of random swell and sea from a natural beach can be roughly parameterized by M.

Frequency–directional spectra, $E(f, \theta)$, estimated from the array data using a variational technique (Herbers and Guza 1990) are shown in Figs. 6a and 7a for two case studies. In the first case (Fig. 6a), $E(f, \theta)$ is narrow in both frequency and direction, and about 8% of the total swell–sea energy is reflected. In the second case study, the incident spectrum is bimodal with roughly equally energetic peaks at 0.07 and 0.11 Hz (Fig. 7a). The reflection of the 0.07 Hz swell ($R^2 \sim 0.3$) is significantly greater than that of the 0.11 Hz waves ($R^2 \sim 0.2$) (Fig. 7b). On both occasions (and other cases not shown) the spectra of seaward propagating waves, $E_{off}(f)$, retain much of the structure of

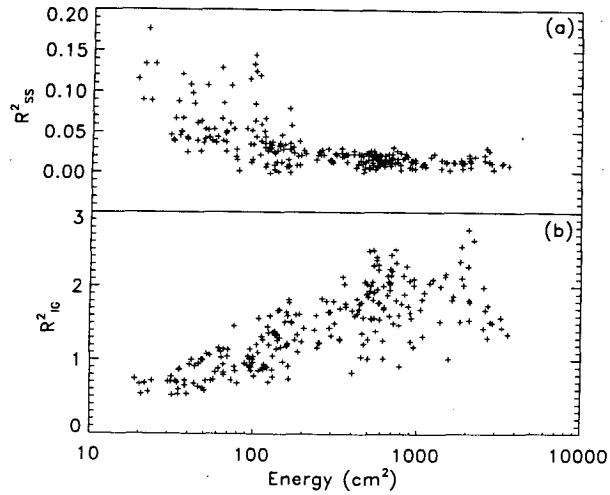

FIG. 3. Ratio of seaward to shoreward propagating energy vs energy in the swell–sea frequency band. (a) Swell–sea (R^2_{ss}) and (b) infragravity (R^2_{ig}) frequency bands.

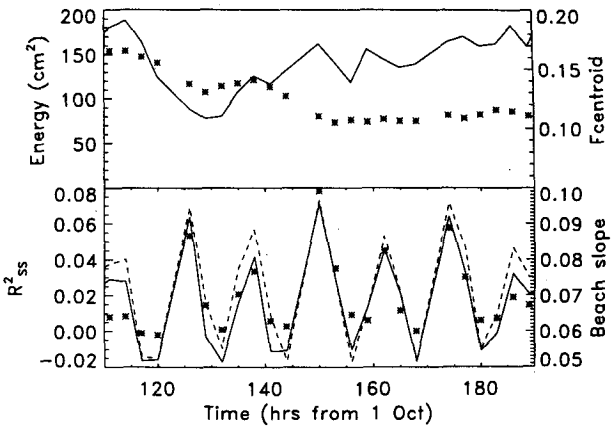

FIG. 4. Swell–sea energy (solid line, upper panel), centroidal frequency (symbols, upper panel), bulk reflection of swell–sea (R^2_{ss}) (symbols, lower panel), beach slope (solid line, lower panel), and water depth (dashed line, lower panel) vs time. The water depth ranged from approximately 12.5 to 14.0 m (scale not shown). The data were obtained 5–8 October 1990.

$E_{on}(f)$ (Figs. 6c and 7c), similar to field observations reported by Tatavarti et al. (1988) and laboratory studies by Kobayashi et al. (1990).

The observed mean propagation directions of shoreward [$\theta_{on}(f)$] and seaward [$\theta_{off}(f)$] traveling waves, defined as

$$\theta_{on}(f) = \frac{\int_{180°}^{360°} \theta E(f, \theta) d\theta}{\int_{180°}^{360°} E(f, \theta) d\theta}, \quad (4a)$$

$$\theta_{off}(f) = \frac{\int_{0°}^{180°} \theta E(f, \theta) d\theta}{\int_{0°}^{180°} E(f, \theta) d\theta}, \quad (4b)$$

are shown in Figs. 6a and 7a. Specularly reflected waves have an angle of propagation in the seaward direction that is equal to the incident angle, reflected about the beach normal. Thus (assuming the reflection coefficient does not vary appreciably with θ), $\theta_{off}(f) \approx 360° - \theta_{on}(f)$ for specular reflection, qualitatively consistent with the observed $\theta_{off}(f)$ (Figs. 6a, 7a, and other cases not shown).

b. *Infragravity waves*

In contrast to R^2_{ss}, R^2_{ig} is often greater than 1 (Fig. 2b), indicating that seaward propagating waves dominate the infragravity frequency band. Furthermore, R^2_{ig} increases from 0.5–1 for wave fields with low total swell–sea energy to 1–3 for wave fields with high swell–sea energy (Fig. 3b), as opposed to the observed decrease in R^2_{ss} (Fig. 3a). Clearly, the interpretation of R^2 is different for the swell–sea and infragravity frequency bands. A plausible explanation for $R^2_{ig} > 1$ is that free infragravity waves are generated shoreward of the array (e.g., within the surf zone) and radiated seaward, unlike swell and sea, which are primarily generated by wind seaward of the array and dissipated in the surf zone. If all the infragravity energy was generated close to shore and either radiated into deep water or dissipated on the shelf, then $E_{on}(f) = 0$ and $R^2_{ig} \to \infty$.

Shoreward propagating forced infragravity waves, locally excited by nonlinear interactions of swell–sea waves, will reduce R^2_{ig}, but their contribution to the infragravity wave energy is small (<10%) for the field data discussed here (Herbers et al. 1994b). The observed $R^2_{ig} \leq 3$ suggest that a significant fraction of the

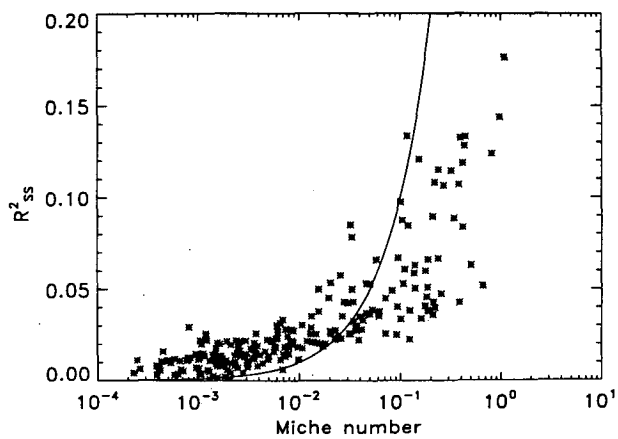

FIG. 5. Bulk reflection of swell–sea (R^2_{ss}) vs the Miche number M. The solid line is $R^2_{ss} = M$ [Eq. (1b)].

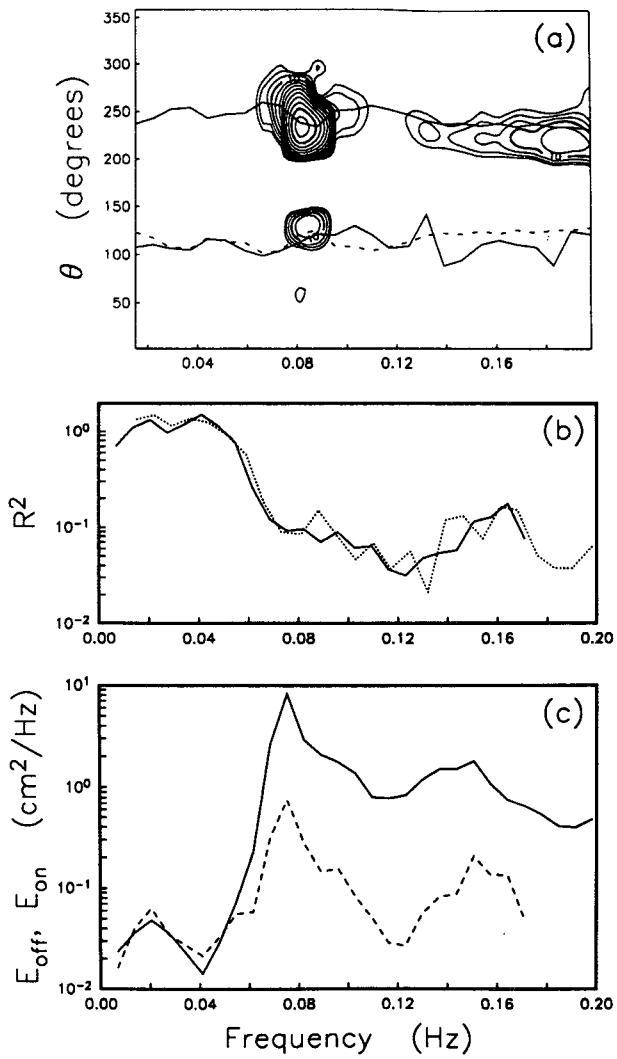

FIG. 6. (a) Contours of the frequency–directional spectrum $E(f, \theta)$ (cm^2/Hz/deg). The mean directions of shoreward- [$\theta_{on}(f)$] and seaward- [$\theta_{off}(f)$] traveling waves [Eq. (4)] are indicated by solid lines. The dashed line is the specular image of $\theta_{on}(f)$. (b) The $R^2(f)$ estimate [appendix and Eq. (2)] (solid line) and an alternative estimate obtained by integrating $E(f, \theta)$ (dotted line). (c) $E_{on}(f)$ (solid line) and $E_{off}(f)$ (dashed line). The data were taken at 0700–0950 EST 6 October 1990 and correspond to the highest R^2_{ss} in Fig. 4: $R^2_{ss} = 0.08$, centroidal frequency: 0.11 Hz, significant wave height: 51 cm, and $\beta = 0.10$.

infragravity energy does not radiate to deep water, but is refractively trapped seaward of the array. Indeed, previous studies have shown the importance of low-mode edge waves in the surf zone (Huntley et al. 1981; Oltman-Shay and Guza 1987; and many others), and significant refractive trapping of infragravity energy between 8-m and 13-m depth at the Duck, North Carolina, experiment site is evident in observed cross-shore energy variations (Herbers et al. 1994b). Consistent with these observations, the directional distributions of infragravity energy in 13-m depth are typically very broad, with a maximum corresponding to alongshore propagation, in contrast to the directionally narrow and primarily shoreward-directed swell (Fig. 8).

When infragravity waves are generated shoreward of the array (e.g., in the surf zone), the ratio of E_{off}/E_{on} is independent of energy losses shoreward of the array, but increases with increasing energy losses on the shelf seaward of the array. These losses could result from dissipation or radiation to the deep ocean. The damping of any particular frequency–directional wave component by bottom friction on the shelf (i.e., seaward of the array) is believed to be nonlinearly proportional to the total velocity (i.e., including all frequencies and directions) at the seafloor (Hasselmann and Collins 1968; Collins 1972). Thus, the relative importance of infragravity wave damping by bottom fric-

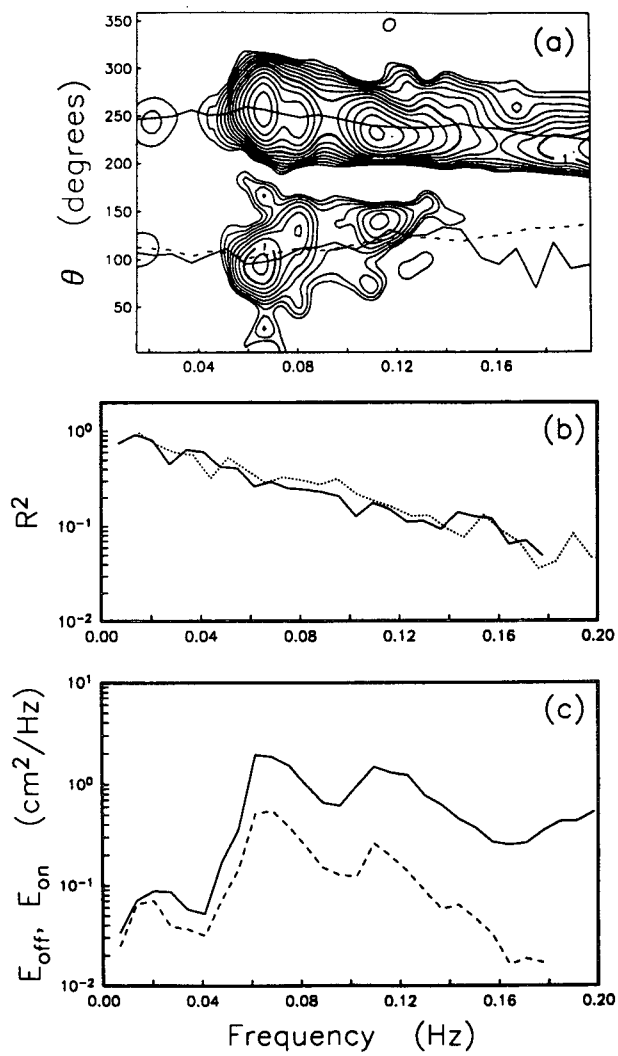

FIG. 7. Same format as Fig. 6. The data were taken at 0400–0650 EST 17 November 1990 and correspond to the maximum observed R^2_{ss}: $R^2_{ss} = 0.18$, centroidal frequency: 0.11 Hz, significant wave height: 19 cm, and $\beta = 0.13$.

tion is expected to increase as the overall wave energy increases, qualitatively consistent with the observed increase in R^2_{ig} (Fig. 3b). Much of the 50-km wide shelf near the North Carolina coast is 20–30 m deep, and relatively short wavelength sea is attenuated at the seafloor. Thus, if bottom friction is important, a higher correlation of R^2_{ig} with swell than with sea energy is expected, consistent with the observations (Fig. 9). However, the trend in the ratio E_{off}/E_{on} (Fig. 3b) could also be caused by increased radiation of infragravity energy to the deep ocean during storms. Although the present observations support the hypothesis that infragravity energy is predominantly generated in very shallow water and radiated seaward, the processes that reduce the efficiency of refractive trapping as the total wave energy increases are not understood.

4. Conclusions

The reflection of ocean surface gravity waves from a natural beach was investigated using measurements from an array of bottom-mounted pressure sensors in 13-m water depth 2 km from the North Carolina coast. The observed ratio of seaward to shoreward propagating energy in the swell–sea frequency band (0.044–0.20 Hz) decreases with increasing wave frequency (Fig. 2b) and increasing wave energy (Fig. 3a), and increases with increasing beach slope (Fig. 4), qualitatively consistent with a parameterization by Miche (1951) (Fig. 5). Observed frequency–directional spectra suggest that the swell–sea reflection is specular (Figs. 6a, 7a). As much as 18% of the shoreward propagating swell–sea energy was reflected at the beach face, but frequently the seaward propagating energy was undetectable (less than 3% of the shoreward propagating energy). In contrast, there was usually more seaward than shoreward propagating energy in the infragravity frequency band (0.010–0.044 Hz), with the relative amount of seaward propagating energy largest for high-energy swell wave fields (Figs. 3b and 9). This trend suggests that infragravity waves, generated in very shallow water, and refractively trapped during seaward propagation over a sloping seabed, are significantly dissipated on the shelf when the swell energy is high.

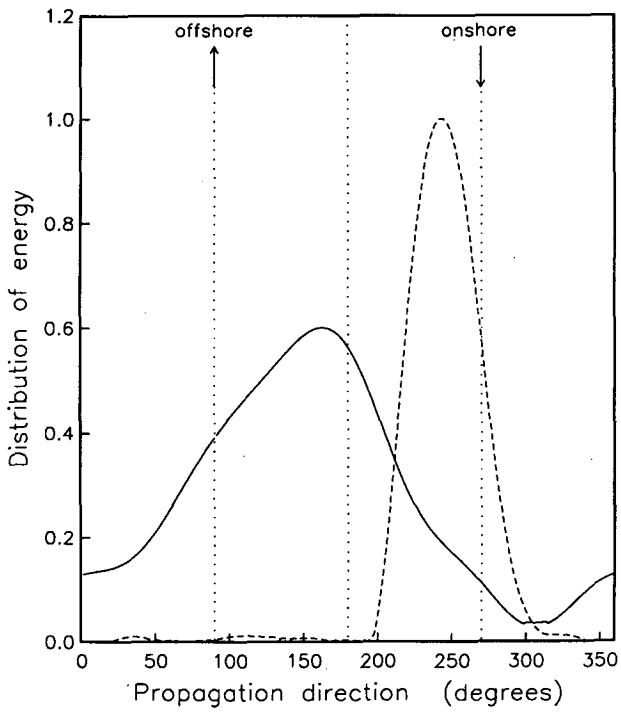

FIG. 8. Directional distribution of swell (dashed line) and infragravity (solid line) energy observed at 1900–2150 EST 11 October 1990. Shoreward propagating waves (180°–360°) account for 98% and 33% of the swell and infragravity energy, respectively. See Herbers et al. 1994b for further details.

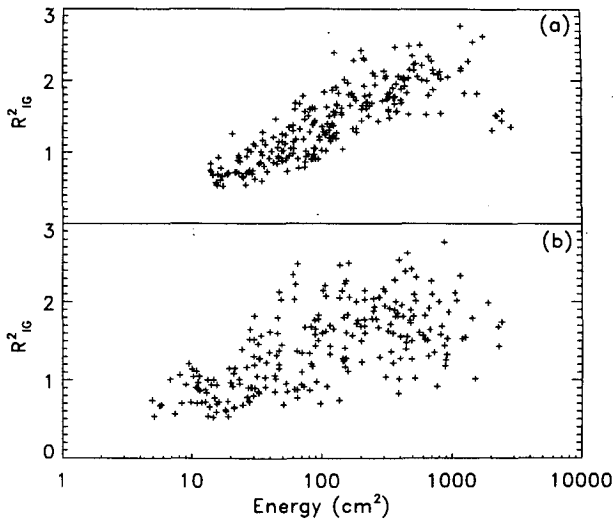

FIG. 9. R^2_{ig} vs (a) energy in the swell frequency band ($0.044 < f < 0.12$ Hz) and (b) energy in the sea frequency band ($0.12 < f < 0.20$ Hz).

Acknowledgments. This research was funded by the Office of Naval Research (Coastal Sciences and Nonlinear Ocean Waves ARI) and the National Science Foundation (Physical Oceanography). Staff from the Center for Coastal Studies, Scripps Institution of Oceanography, deployed and maintained the array. The excellent logistical support provided by the U.S. Army Corps of Engineers Field Research Facility, Duck, North Carolina, is gratefully acknowledged.

APPENDIX

Estimation of $E_{off}(f)$ and $E_{on}(f)$

The cross-spectrum $H_{nm}(f)$ of two bottom-mounted pressure sensors n and m with horizontal space coordinates $\mathbf{x}_n$ and $\mathbf{x}_m$, respectively, is related to the frequency (f)–directional (θ) wave spectrum $E(f, \theta)$ by (e.g., Barber 1963)

$$H_{nm}(f) = \int_0^{2\pi} d\theta \frac{\exp[i\mathbf{k}\cdot(\mathbf{x}_m - \mathbf{x}_n)]}{\cosh^2(kh)} E(f,\theta), \quad \text{(A1)}$$

where h is the water depth and $\mathbf{k} = [k\cos\theta, k\sin\theta]$ is the vector wavenumber with k given by the linear dispersion relation

$$(2\pi f)^2 = gk\tanh(kh) \quad \text{(A2)}$$

and g denotes the acceleration of gravity. Equation (A1) can be expressed in the general form (dropping the frequency dependence)

$$\mathbf{d} = \int_0^{2\pi} d\theta \mathbf{b}(\theta) E(\theta), \quad \text{(A3)}$$

where the elements of the true (i.e., error-free) data vector $\mathbf{d}$ are the auto-, co-, and quadrature-spectra, and the corresponding elements of the kernel vector $\mathbf{b}(\theta)$ are known functions of the sensor positions and the wave frequency and propagation direction [Eqs. (A1), (A2)]. The energy density $E_{\text{off}}(f)$ of seaward traveling waves [Eq. (2c)] can be written as

$$E_{\text{off}} = \int_0^{2\pi} d\theta H(\theta) E(\theta) \quad \text{(A4)}$$

with

$$H(\theta) \equiv \begin{cases} 1, & \text{if } 0 < \theta \leq \pi; \\ 0, & \text{if } \pi < \theta \leq 2\pi. \end{cases} \quad \text{(A5)}$$

The estimate $\hat{E}_{\text{off}}$ of E_{off} is expressed as a linear sum of the cross-spectra (Davis and Regier 1977; Pawka et al. 1983; and many others):

$$\hat{E}_{\text{off}} \equiv \boldsymbol{\lambda}^{\mathrm{T}}\tilde{\mathbf{d}}. \quad \text{(A6)}$$

Here $\tilde{\mathbf{d}}$ is the observed data vector and the elements of $\boldsymbol{\lambda}$ are the cross-spectral weights. The estimated $\hat{E}_{\text{off}}$ is related to the true E_{off} by [Eqs. (A3), (A4), (A6)]:

$$\hat{E}_{\text{off}} = E_{\text{off}} + \int_0^{2\pi} d\theta[\boldsymbol{\lambda}^{\mathrm{T}}\mathbf{b}(\theta) - H(\theta)]E(\theta) + \boldsymbol{\lambda}^{\mathrm{T}}(\tilde{\mathbf{d}} - \mathbf{d}), \quad \text{(A7)}$$

where the second and third terms on the right-hand side are errors in the estimate owing to the limited array resolution $[\boldsymbol{\lambda}^{\mathrm{T}}\mathbf{b}(\theta) \neq H(\theta)]$ and statistical uncertainty in the observations ($\tilde{\mathbf{d}} \neq \mathbf{d}$), respectively.

Elements of $\boldsymbol{\lambda}$ may be chosen such that the window $\boldsymbol{\lambda}^{\mathrm{T}}\mathbf{b}(\theta)$ closely resembles $H(\theta)$, and $\hat{E}_{\text{off}}$ is approximately unbiased. However, this will generally yield large values for the elements of $\boldsymbol{\lambda}$ and estimates of E_{off} that are very sensitive to errors in the data vector $\mathbf{d}$ [Eq. (A7)]. Conversely, statistical scatter in $\hat{E}_{\text{off}}$ may be reduced by making $|\boldsymbol{\lambda}|$ small, but at the expense of a larger bias. To find an appropriate balance between bias and sensitivity to data errors an error function χ of the form

$$\chi = \int_0^{2\pi} d\theta[\boldsymbol{\lambda}^{\mathrm{T}}\mathbf{b}(\theta) - H(\theta)]^2 + \alpha\mathbf{E}\{[\boldsymbol{\lambda}^{\mathrm{T}}(\tilde{\mathbf{d}} - \mathbf{d})]^2\} \quad \text{(A8)}$$

is minimized, where $\mathbf{E}\{\ \}$ denotes the expected value, and α is the trade-off parameter (e.g., Backus and Gilbert 1970; Davis and Regier 1977). Setting $\partial\chi/\partial\boldsymbol{\lambda} = 0$ yields a linear system of equations for the elements of $\boldsymbol{\lambda}$:

$$[\mathbf{C} + \alpha\mathbf{V}]\boldsymbol{\lambda} = \int_0^{2\pi} d\theta \mathbf{b}(\theta) H(\theta), \quad \text{(A9)}$$

where the matrices $\mathbf{C}$ and $\mathbf{V}$ are defined as

$$\mathbf{C} \equiv \int_0^{2\pi} d\theta \mathbf{b}(\theta)\mathbf{b}^{\mathrm{T}}(\theta), \quad \text{(A10a)}$$

$$\mathbf{V} \equiv \mathbf{E}\{(\tilde{\mathbf{d}} - \mathbf{d})(\tilde{\mathbf{d}} - \mathbf{d})^{\mathrm{T}}\}. \quad \text{(A10b)}$$

Whereas the matrix $\mathbf{C}$ is a function only of the wave frequency f, the water depth h, and the array geometry, the error covariance matrix $\mathbf{V}$ depends on the true values of the cross-spectra (e.g., Jenkins and Watts 1968):

$$\mathbf{E}\{(\tilde{H}_{pq} - H_{pq})(\tilde{H}_{rs} - H_{rs})\} = \frac{2}{\nu} H_{ps}H_{rq}, \quad \text{(A11)}$$

with ν the number of degrees of freedom of the observed cross-spectra $\tilde{H}_{nm}$. For the present case of large ν, accurate estimates of the elements of $\mathbf{V}$ are obtained by substituting the observed $\tilde{H}_{nm}$ in the right-hand side of Eq. (A11) (Davis and Regier 1977). Measurement errors (i.e., calibration inaccuracies and digitization noise) are relatively small and are neglected here.

Substitution of $\boldsymbol{\lambda}$ [Eq. (A9)] in Eq. (A6) yields an estimate of the energy density $E_{\text{off}}(f)$ of seaward traveling waves at frequency f. The energy density $E_{\text{on}}(f)$ of shoreward traveling waves follows simply by taking the difference of the (total) observed energy density $\hat{E}(f)$ [estimated by taking the average of the autospectra corrected to surface elevation, Eq. (A1)] and $\hat{E}_{\text{off}}(f)$.

The accuracy of $R^2(f)$ [$= \hat{E}_{\text{off}}(f)/\hat{E}_{\text{on}}(f)$] estimates was verified through model tests with simulated array data. In each test, 16 random realizations of cross-spectra $\tilde{H}_{nm}$ were generated for the Duck 13-m depth array geometry (Fig. 1a) for a specified wave frequency f and directional spectrum $E(\theta)$. Estimated and true R^2 were compared for different f, $E(\theta)$, ν, and α. The model tests indicate a weak sensitivity of the estimates to the value of the trade-off parameter α, unless there is a gross imbalance between the weighting of array bias and statistical scatter [i.e., when $\alpha E^2 \ll 1$ or $\alpha E^2 \gg 1$, Eqs. (A7), (A8)]. A value of $\alpha = 0.25/\hat{E}^2$ was used for all estimates presented here. Examples of model test results for 0.1 Hz (swell) and 0.02 Hz (infragravity) waves are shown in Fig. A1. The $E(\theta)$ and degrees of freedom ($\nu = 500$) used in these simulations are roughly representative of the observed $E(\theta)$ (Figs.

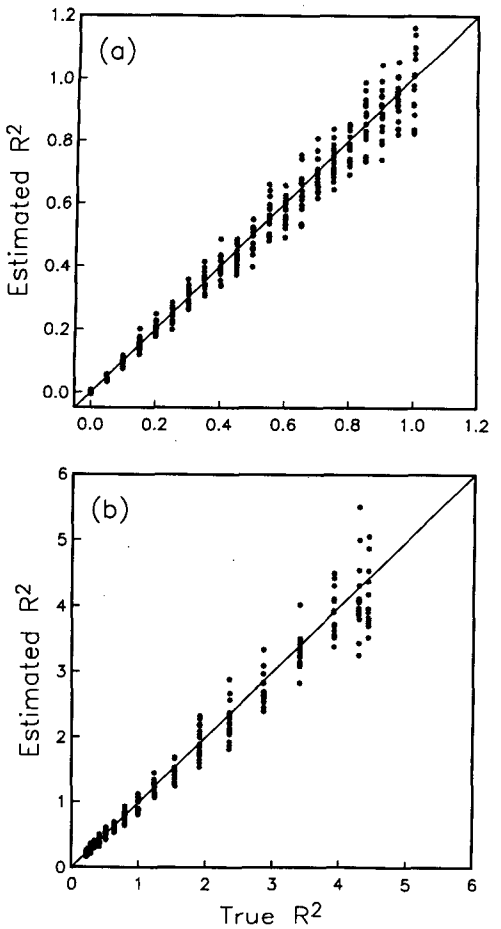

FIG. A1. Estimated vs true R^2 obtained from simulations. (a) Directionally narrow 0.1-Hz swell with $E(\theta) \propto R^2 \cos^{80}[(\theta - 120°)/2] + \cos^{80}[(\theta - 240°)/2]$. (b) Directionally broad 0.02-Hz infragravity waves with $E(\theta) \propto \cos^2[(\theta - \theta_{mean})/2]$ (mean propagation directions θ_{mean} ranging from offshore to onshore are included).

6a, 7a, and 8) and the degrees of freedom in the measurements [integrated over the swell–sea and infragravity bands, Eq. (3)]. At swell–sea frequencies the bias and variance of the R^2 estimates are small (e.g., Fig. A1a) and reflections as weak as $R^2 = 0.05$ are unambiguously detected by the array. At infragravity frequencies the R^2 estimates are somewhat degraded by the limited array aperture (less than a wavelength), but the directional spectra observed at infragravity frequencies are generally broader than the swell–sea directional spectra (e.g., Fig. 8) and span a wide range of R^2 that is well resolved by the measurements (Fig. A1b).

Alternatively $E_{off}(f)$ and $E_{on}(f)$ may be determined by integrating estimates of $E(f, \theta)$ [Eqs. (2b) and (2c)]. This indirect approach was not pursued here because it does not allow for an optimal trade-off between bias and stability of R^2 estimates. Nevertheless, estimates of $R^2(f)$ obtained by integrating the observed $E(f, \theta)$ for a few selected case studies are in good agreement with the estimates obtained directly from the cross-spectra (e.g., Figs. 6b, 7b).

REFERENCES

Backus, G., and F. Gilbert, 1970: Uniqueness in the inversion of inaccurate gross earth data. *Philos. Trans. Roy. Soc. London A,* **266,** 123–192.

Barber, N. F., 1963: The directional resolving power of an array of wave detectors. *Ocean Wave Spectra,* Prentice-Hall, 137–150.

Birkemeier, W., K. Hathaway, J. Smith, C. Baron, and M. Leffler, 1992: DELILAH Experiment: Investigator's summary report. US Army Corps of Engineers, 220 pp.

Carrier, G. F., and H. P. Greenspan, 1958: Water waves of finite amplitude on a sloping beach. *J. Fluid Mech.,* **4,** 97–109.

Collins, J. I., 1972: Prediction of shallow-water spectra. *J. Geophys. Res.,* **77,** 2693–2707.

Davis, R. E., and L. A. Regier, 1977: Methods for estimating directional wave spectra from multi-element arrays. *J. Mar. Res.,* **35,** 453–477.

Elgar, S., T. H. C. Herbers, M. Okihiro, J. Oltman-Shay, and R. T. Guza, 1992: Observations of infragravity waves. *J. Geophys. Res.,* **97,** 15 573–15 577.

Freilich, M. H., and R. T. Guza, 1984: Nonlinear effects on shoaling surface gravity waves. *Philos. Trans. Roy. Soc. London A,* **311,** 1–41.

Guza, R. T., and A. J. Bowen, 1976: Resonant interactions for waves breaking on a beach. *Proc. 15th Int. Coastal Engineering Conf.,* Honolulu, ASCE, 560–579.

——, and E. B. Thornton, 1985: Observations of surf beat. *J. Geophys. Res.,* **90,** 3161–3172.

——, ——, and R. A. Holman, 1984: Swash on steep and shallow beaches. *Proc. 19th Int. Coastal Engineering Conf.,* Houston, ASCE, 708–723.

Hasselmann, K., and J. I. Collins, 1968: Spectral dissipation of finite-depth gravity waves due to bottom friction. *J. Mar. Res.,* **26,** 1–26.

Herbers, T. H. C., and R. T. Guza, 1990: Estimation of directional wave spectra from multicomponent observations. *J. Phys. Oceanogr.,* **20,** 1703–1724.

——, S. Elgar, and R. T. Guza, 1994a: Infragravity frequency (0.005–0.05 Hz) motions on the shelf. Part I: Forced waves. *J. Phys. Oceanogr.,* **24,** 917–927.

——, S. Elgar, R. T. Guza, and W. C. O'Reilly, 1994b: Infragravity frequency (0.005–0.05 Hz) motions on the shelf. Part II: Free waves. *J. Phys. Oceanogr.,* submitted.

Huntley, D., R. T. Guza, and E. B. Thornton, 1981: Field observations of surf beat. 1. Progressive edge waves. *J. Geophys. Res.,* **86,** 6451–6466.

Jenkins, G. M., and D. M. Watts, 1968: *Spectral Analysis and Its Applications.* Holden-Day, 525 pp.

Kirby, J. T., 1986: A general wave equation over rippled beds. *J. Fluid Mech.,* **162,** 171–186.

——, 1987: A program for calculating the reflectivity of beach profiles. University of Florida Report UFL/COEL-87/004.

Kobayashi, N., D. Cox, and A. Wurjanto, 1990: Irregular wave reflection and run-up on rough impermeable slopes. *ASCE J. Waterw., Harbors, Coastal Eng. Div.,* **116,** 708–726.

Mansard, E. P. D., and E. R. Funke, 1980: The measurement of incident and reflected spectra using a least squares method. *Proc. 17th Int. Conf. on Coastal Eng.,* Sydney, ASCE, 154–172.

Meyer, R. E., and A. D. Taylor, 1972: Runup on beaches. *Waves on Beaches,* R. E. Meyer, Ed., Academic Press, 357–411.

Miche, M., 1951: Le pouvoir reflechissant des ouvrages maritimes exposes a l'action de la houle. *Ann. Points. Chaussees,* **121,** 285–319.

Moraes, C., 1970: Experiments of wave reflection on impermeable slopes. *Proc. 12th Int. Conf. Coastal Eng.,* Washington, DC, ASCE, 509–521.

Munk, W. H., and M. Wimbush, 1969: A rule of thumb for breaking over sloping beaches. *Oceanology,* **9,** 56–59.

Nelson, R. C., and J. Gonsalves, 1990: A field study of reflections from an exposed dissipative beach. *Coastal Eng.,* **14,** 457–477.

Okihiro, M., R. T. Guza, and R. J. Seymour, 1992: Bound infragravity waves. *J. Geophys. Res.,* **97,** 11 453–11 469.

Oltman-Shay, J., and R. T. Guza, 1987: Infragravity edge wave observations on two California beaches. *J. Phys. Oceanogr.,* **17,** 644–663.

Pawka, S. S., D. L. Inman, and R. T. Guza, 1983: Radiation stress estimators. *J. Phys. Oceanogr.,* **13,** 1698–1708.

Suhayda, J. N., 1974: Standing waves on beaches. *J. Geophys. Res.,* **72,** 3065–3071.

Tatavarti, V., D. Huntley, and A. J. Bowen, 1988: Incoming and seaward going wave interactions on beaches. *Proc. 21st Int. Conf. on Coastal Engineering,* Malaga, Spain, ASCE, 136–150.

Walton, T. L., 1992: Wave reflection from natural beaches. *Ocean Eng.,* **19,** 239–258.